Altered biometal homeostasis is associated with CLN6 mRNA loss in mouse neuronal ceroid lipofuscinosis

Katja M. Kanninen[1,*,‡], Alexandra Grubman[1,‡], Aphrodite Caragounis[1], Clare Duncan[1], Sarah J. Parker[1,*], Grace E. Lidgerwood[1], Irene Volitakis[2], George Ganio[2], Peter J. Crouch[1] and Anthony R. White[1,§]

[1]Department of Pathology, The University of Melbourne, Parkville, Victoria 3010, Australia
[2]Florey Institute of Neuroscience and Mental Health, The University of Melbourne, Parkville, Victoria 3010, Australia

*Present address: AI Virtanen Institute for Molecular Sciences, University of Eastern Finland, Kuopio 70211, Finland
‡These authors contributed equally to this work
§Author for correspondence (arwhite@unimelb.edu.au)

Biology Open 2, 635–646
doi: 10.1242/bio.20134804
Received 15th March 2013
Accepted 23rd April 2013

Summary

Neuronal ceroid lipofuscinoses, the most common fatal childhood neurodegenerative illnesses, share many features with more prevalent neurodegenerative diseases. Neuronal ceroid lipofuscinoses are caused by mutations in CLN genes. CLN6 encodes a transmembrane endoplasmic reticulum protein with no known function. We characterized the behavioural phenotype of spontaneous mutant mice modeling CLN6 disease, and demonstrate progressive motor and visual decline and reduced lifespan in these mice, consistent with symptoms observed in neuronal ceroid lipofuscinosis patients. Alterations to biometal homeostasis are known to play a critical role in pathology in Alzheimer's, Parkinson's, Huntington's and motor neuron diseases. We have previously shown accumulation of the biometals, zinc, copper, manganese and cobalt, in CLN6 Merino and South Hampshire sheep at the age of symptom onset. Here we determine the physiological and disease-associated expression of CLN6, demonstrating regional CLN6 transcript loss, and concurrent accumulation of the same biometals in the CNS and the heart of presymptomatic CLN6 mice. Furthermore, increased expression of the ER/Golgi-localized cation transporter protein, Zip7, was detected in cerebellar Purkinje cells and whole brain fractions. Purkinje cells not only control motor function, an early symptomatic change in the CLN6 mice, but also display prominent neuropathological changes in mouse models and patients with different forms of neuronal ceroid lipofuscinoses. Whole brain fractionation analysis revealed biometal accumulation in fractions expressing markers for ER, Golgi, endosomes and lysosomes of CLN6 brains. These data are consistent with a link between CLN6 expression and biometal homeostasis in CLN6 disease, and provide further support for altered cation transporter regulation as a key factor in neurodegeneration.

Key words: Neurodegeneration, Biometal homeostasis, Neuronal ceroid lipofuscinoses, CLN6, Metal transporter

Introduction

Neuronal ceroid lipofuscinoses (NCLs), the most common childhood neurodegenerative illnesses, are a group of fatal, autosomal recessive lysosomal storage disorders, with many features in common with more prevalent neurodegenerative diseases, including oxidative stress, neuroinflammation and protein aggregation (reviewed by Jalanko and Braulke, 2009). There are at least eleven forms of NCLs which all share common pathological features and clinical symptoms, but are distinguished by the age of onset and genetic deficit (Kousi et al., 2012). Currently, there is little understanding of how genetic mutations in proteins such as CLN6, the cause of variant late infantile NCL (Sharp et al., 1997), result in CLN6 disease, characterized by selective and regional neuronal cell degeneration.

CLN6 is a transmembrane endoplasmic reticulum (ER) protein with no known function and no homologous proteins in NCBI, Ensembl or other protein databases (Mole et al., 2004). Mutations in the CLN6 gene result in disease clinically characterized by seizures, vision impairment and motor dysfunction and premature death. To date, 63 disease-associated mutations have been identified in CLN6 (Kousi et al., 2012), which map to ER lumen or transmembrane residues. One of the mutations identified in the CLN6 gene causes a frameshift and premature stop codon. This identical mutation has been identified in B6.Cg-*Cln6nclf*/J (CLN6) mice, a naturally occurring model for NCL disease (Gao et al., 2002). While the behavioral phenotype of the CLN6 mice remains poorly characterized, this model displays pathological features such as brain atrophy and inflammation (Thelen et al., 2012b), closely resembling the disease in humans (Bronson et al., 1998).

Deregulation of transition metal homeostasis is a pathological feature common to multiple neurodegenerative disorders (reviewed by Bolognin et al., 2009). Specifically, altered homeostasis of zinc, an essential enzyme co-factor with physiological functions in synaptic transmission has been repeatedly associated with neurodegeneration. Metal transporter proteins, including members of the Zip/SLC39A cation influx and ZnT/SLC30A cation efflux protein families, primarily control intracellular biometal distribution. Alterations in these

transporters are associated with deregulation of metal homeostasis in Parkinsonism, Alzheimer's and the lysosomal storage disease Mucolipidosis Type IV (Lovell et al., 2005; Lyubartseva et al., 2010; Kiselyov et al., 2011; Beyer et al., 2012; Quadri et al., 2012). We have recently shown that biometal homeostasis is also altered in ovine CLN6 disease (Kanninen et al., 2013). In particular, zinc and manganese accumulate in the brain regions of CLN6 affected sheep where neuroinflammation and neurodegeneration first occur.

In this study we demonstrate that the CLN6 mice displayed progressive motor and visual decline and a reduced lifespan, all of which are features in common with NCL patients. We determined that CLN6 transcript loss was associated with altered biometal homeostasis in CNS tissues, but also in the heart of presymptomatic CLN6 mice. Furthermore, alterations to the cation transporter protein Zip7 were detected in CLN6 brain areas displaying initial neuropathological changes and biometal accumulation.

Results

CLN6 mice demonstrate reduced lifespan and progressive motor and visual decline

The CLN6 mouse (Bronson et al., 1998) is a well-established model of variant late infantile NCL, although the behavioural phenotype has not been extensively studied. To investigate the onset and development of motor and visual symptoms in CLN6 mice, we performed behavioural analyses from the age of 14 weeks on a cohort of 22 control and 24 CLN6 affected mice. The life span of CLN6 mutant mice was significantly reduced compared to control littermates (Fig. 1A, $P<0.0001$). Control mice were healthy at the end of the study at 54 weeks of age, whereas CLN6 animals displayed a median survival of 46 weeks. While CLN6 mice began to lose weight from approximately 23 weeks of age, control mice steadily gained weight over the course of the study (Fig. 1B, $P=0.0029$ for effect of genotype).

Weekly visual placement and grip strength tests were performed to assess visual and motor functions, respectively. Additionally, mice were subjected to accelerating rotarod analyses as a measure of balance and motor coordination. Male mice performed worse on the rotarod and grip tests than female mice for both genotypes and at all ages tested (data not shown). All data presented are pooled male and female mice. Control mice performed well on the rotarod independent of age, with the mean rotarod score not falling lower than 160 seconds at any age. Rotarod performance in CLN6 mice, however, was significantly impaired from 34 weeks of age (Fig. 1C, $P<0.0001$), and progressively declined with age. Similarly, vision and grip strength were significantly impaired in CLN6 mice from an age of 42 and 43 weeks, respectively, whereas no significant changes to visual placing or grip strength were observed in control animals (Fig. 1D, $P<0.0001$ and Fig. 1E, $P=0.0002$, respectively). Taken together, these results indicate that in CLN6 mice, both visual and locomotor functions are drastically impaired and progressively decline over the course of disease.

Spatial and temporal CLN6 transcript loss in CLN6 mice

Currently, there is little understanding of how genetic mutations in CLN6 result in selective and regional neuronal cell degeneration. Regional loss of CLN6 mRNA has been reported

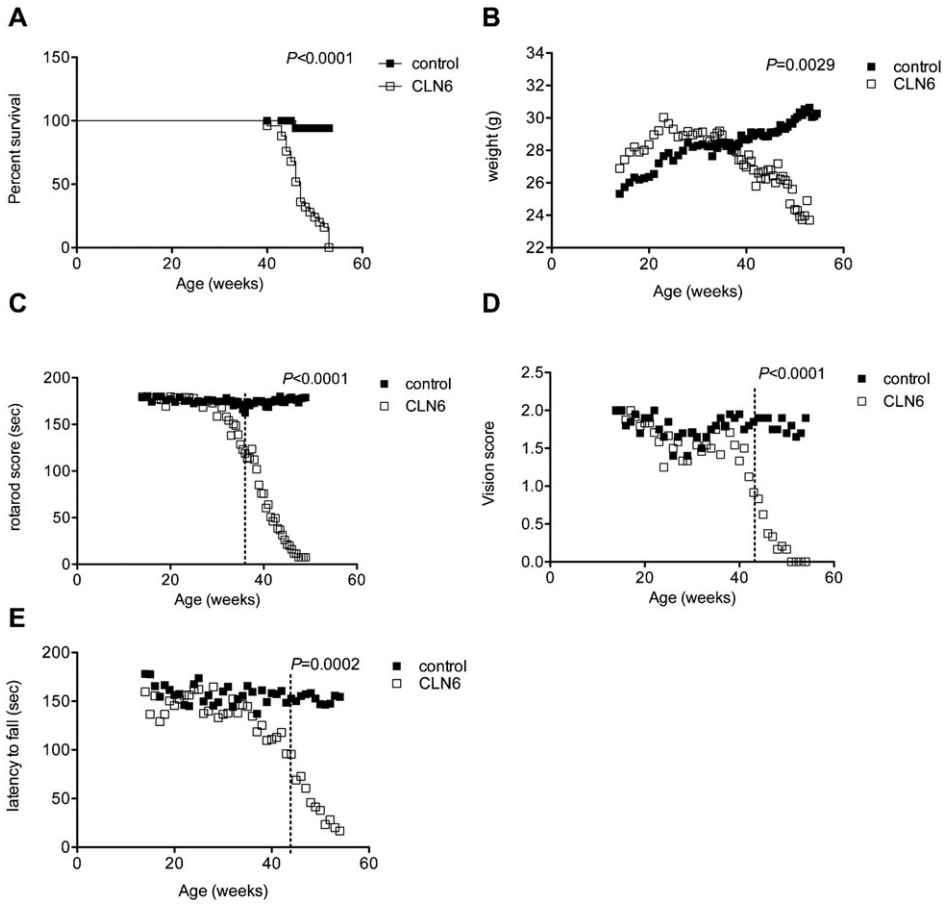

Fig. 1. CLN6 mice demonstrate reduced lifespan and progressive motor and visual decline. (**A**) Survival analysis of CLN6 ($n=24$) and control C57BL/6 littermates ($n=22$). Mice displaying full hind limb paralysis, over 15% weight loss from peak body weight or rotarod performance less than 10 seconds in 2 consecutive trials, were culled in accordance with ethical guidelines. $P<0.0001$ as calculated by the Log-rank (Mantel–Cox) Test. (**B**) CLN6 and control C57BL/6 mice were weighed twice-weekly over the duration of the study. $P=0.0029$ for the effect of genotype on body weight as assessed by 2-way ANOVA. (**C**) Motor function was assessed by rotarod performance. $P<0.0001$ as assessed by 2-way ANOVA. Means became significantly different from the age of 34 weeks as assessed by post-hoc Bonferonni tests. (**D**) Visual function was determined by the visual placing test. Mice were graded on a scale from 0–2. $P<0.0001$ as assessed by 2-way ANOVA. Means became significantly different from the age of 42 weeks as assessed by post-hoc Bonferonni tests. (**E**) Grip strength was assessed weekly by the inverted grid test of grip strength. The longest time taken to fall from 2 consecutive trials each performed for 180 seconds was recorded. $P=0.0002$ as assessed by 2-way ANOVA. Means became significantly different from the age of 43 weeks as assessed by post-hoc Bonferonni tests. For ease of visualization, all data (B–E) are expressed as mean values.

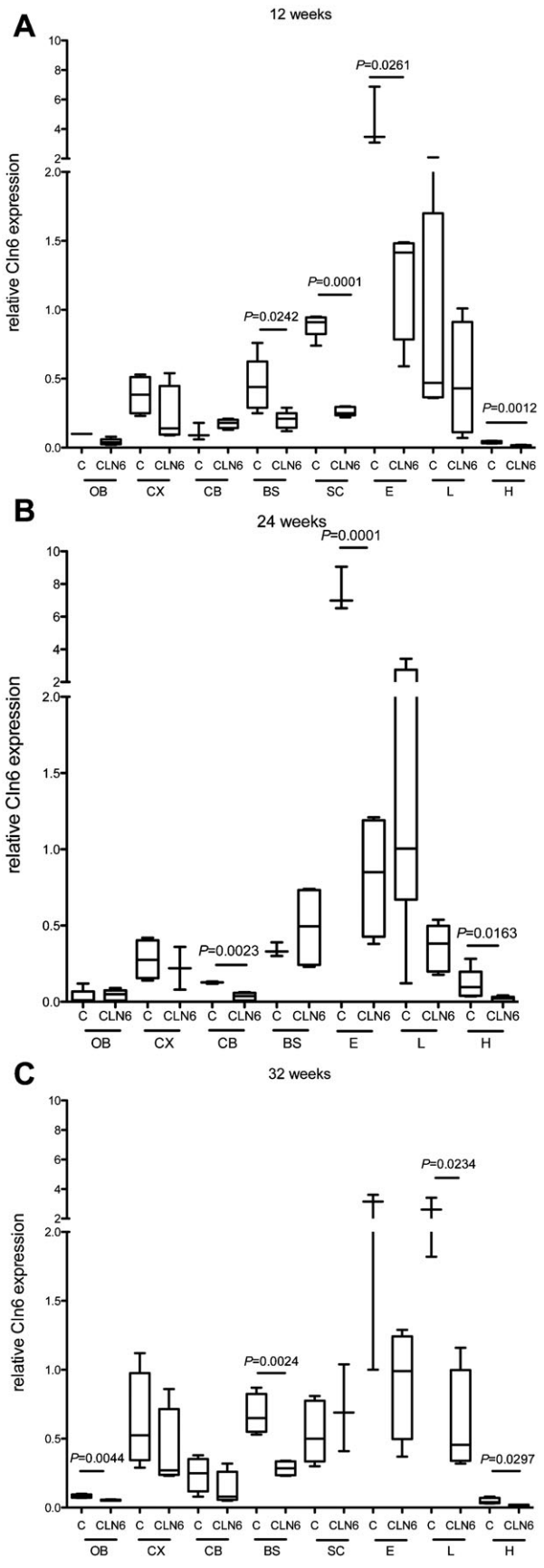

in the cerebellum and hippocampus of day 0 (newborn) CLN6 mice (Thelen et al., 2012a). We therefore hypothesized that investigation of spatio-temporal CLN6 expression levels may provide insight into the physiological function of the CLN6 protein. Using qRT-PCR, we examined the expression of CLN6 mRNA in the CNS and peripheral tissues harvested from control and CLN6 mice (Fig. 2A–C). The age groups corresponding to 12, 24 and 32 weeks of age were selected to represent early presymptomatic, late presymptomatic and symptom onset time points based on rotarod performance, to investigate the relationship between temporal CLN6 transcription and biochemical changes occurring prior to symptom onset. In control mice, CLN6 tissue expression remained consistent over all ages tested. Expression of CLN6 transcripts was significantly reduced in a number of CNS tissues. Specifically, brainstem and spinal cord CLN6 expression levels were substantially lower in CLN6 mice at 12 weeks of age, whereas by 24 weeks of age, CLN6 transcription was specifically decreased in the cerebella of CLN6 mice. At 32 weeks of age, CNS CLN6 expression was reduced in olfactory bulb and brainstem of CLN6 mice.

Consistent with the reported early retinal degeneration observed in CLN6 mice (Bronson et al., 1998), CLN6 expression in the eyes of affected mice was significantly reduced at 12 and 24 weeks of age, with a trend towards reduction at 32 weeks of age. Interestingly, CLN6 expression in the heart was decreased from 12 weeks of age, and remained decreased at all ages tested. Notably, the lowest tissue CLN6 expression was detected in the olfactory bulb, cerebellum and heart. These data indicate the tissues where maintenance of CLN6 expression may be required for physiological functions in motor and visual control, however, analysis of biochemical correlates is required to determine the functional outcomes of lowered CLN6 expression that may contribute to disease progression.

Altered biometal homeostasis is associated with CLN6 transcript loss in pre-symptomatic CLN6 mice

We have previously demonstrated substantial alterations to biometal concentrations in brain tissue isolated from symptomatic CLN6 affected sheep (Kanninen et al., 2013). Given the importance of altered biometal homeostasis to pathology in various neurodegenerative disorders, including Alzheimer's and Parkinson's diseases (Bolognin et al., 2009), we investigated whether biometal accumulation also occurs in presymptomatic CLN6 mice. Assessing the concentrations of 28 metals revealed that 14 were below the limit of detection. Of the remaining 14 metals, significant regional accumulation of the biometals zinc, manganese, cobalt and copper, was detected in presymptomatic CLN6 mice (Fig. 3).

At 12 weeks of age, the most substantial alterations to metal concentrations were observed in the spinal cord. Specifically, zinc, cobalt and copper concentrations were elevated in the spinal cords of CLN6 animals (Fig. 3A,C,D), which was associated with a decrease in CLN6 mRNA expression in these animals

Fig. 2. Spatial and temporal CLN6 transcript loss in CLN6 mice. RNA isolated from CNS and peripheral tissues of 12 (**A**), 24 (**B**) and 32 (**C**) week-old control and CLN6 mice was reverse transcribed to cDNA and analysed for CLN6 transcript expression by qRT-PCR. Values are presented relative to tubulin expression. C, control; OB, olfactory bulb; CX, cortex; CB, cerebellum; BS, brainstem; SC, spinal cord; E, eye; L, liver; H, heart. *P* values determined by Student's *t* test. The box plots represent minimum, 25th percentile, median, 75th percentile and maximum relative expression values.

(Fig. 2A). Other regional increases to biometals were observed in the cortex, liver and heart. CLN6 mouse cortices contained an elevated zinc and copper content (Fig. 3A,D), while zinc and manganese concentrations were increased in the liver (Fig. 3A,B). In the heart, where significant loss of CLN6 mRNA was detected (Fig. 2A), copper concentrations were also significantly elevated (Fig. 3D).

Importantly, there was an inverse relationship between regional CLN6 mRNA expression at 24 weeks and accumulation of biometals in CLN6 mice. Significantly elevated zinc, copper, manganese and cobalt were observed in the cerebellum and heart of CLN6 animals (Fig. 4A–C). Accumulation of these 4 biometals in the heart was still evident by 32 weeks of age (Fig. 5A–D), which was consistent with the sustained reduction in CLN6 mRNA

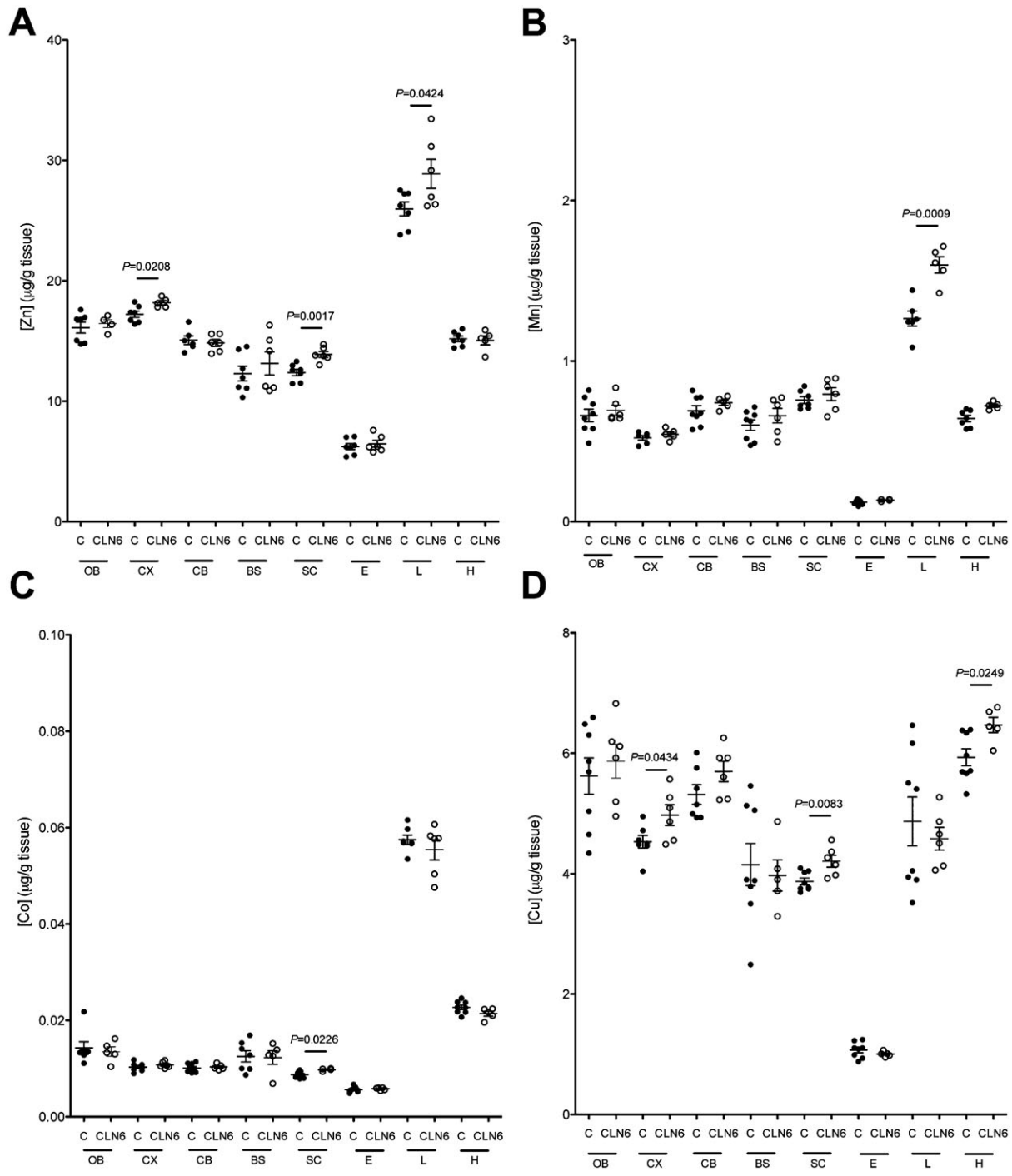

Fig. 3. Biometals accumulate in the spinal cord, cortex, heart and liver of 12 week old CLN6 mice. Metal concentrations in the CNS and peripheral tissues of 12 week old control and mutant CLN6 mice were measured using ICP-MS. The concentrations of zinc (**A**), manganese (**B**), cobalt (**C**) and copper (**D**) in each tissue are expressed as mean±S.D. values. C, control; OB, olfactory bulb; CX, cortex; CB, cerebellum; BS, brainstem; SC, spinal cord; E, eye; L, liver; H, heart. *P* values determined by Student's *t* test.

expression. Interestingly, magnesium, which is known to be important for heart function (Sueta et al., 1995), was also increased in a time-dependent manner in the heart of CLN6 mice (supplementary material Fig. S1). The concentrations of cobalt and copper were also elevated in the cortex of CLN6 mice at 32 weeks of age, and elevated zinc was observed in the spinal cord (Fig. 5A,C,D). Curiously, a significant reduction in copper levels and a trend towards reduction of the other tested metals was observed in the olfactory bulb of 32-week old CLN6 mice, indicating that deregulation of biometals is a complex region-specific process in these mice. Taken together, these data suggest that disruption of biometal homeostasis may be inversely linked to CLN6 expression and precedes detectable disease symptoms in this mouse model of CLN6 NCL.

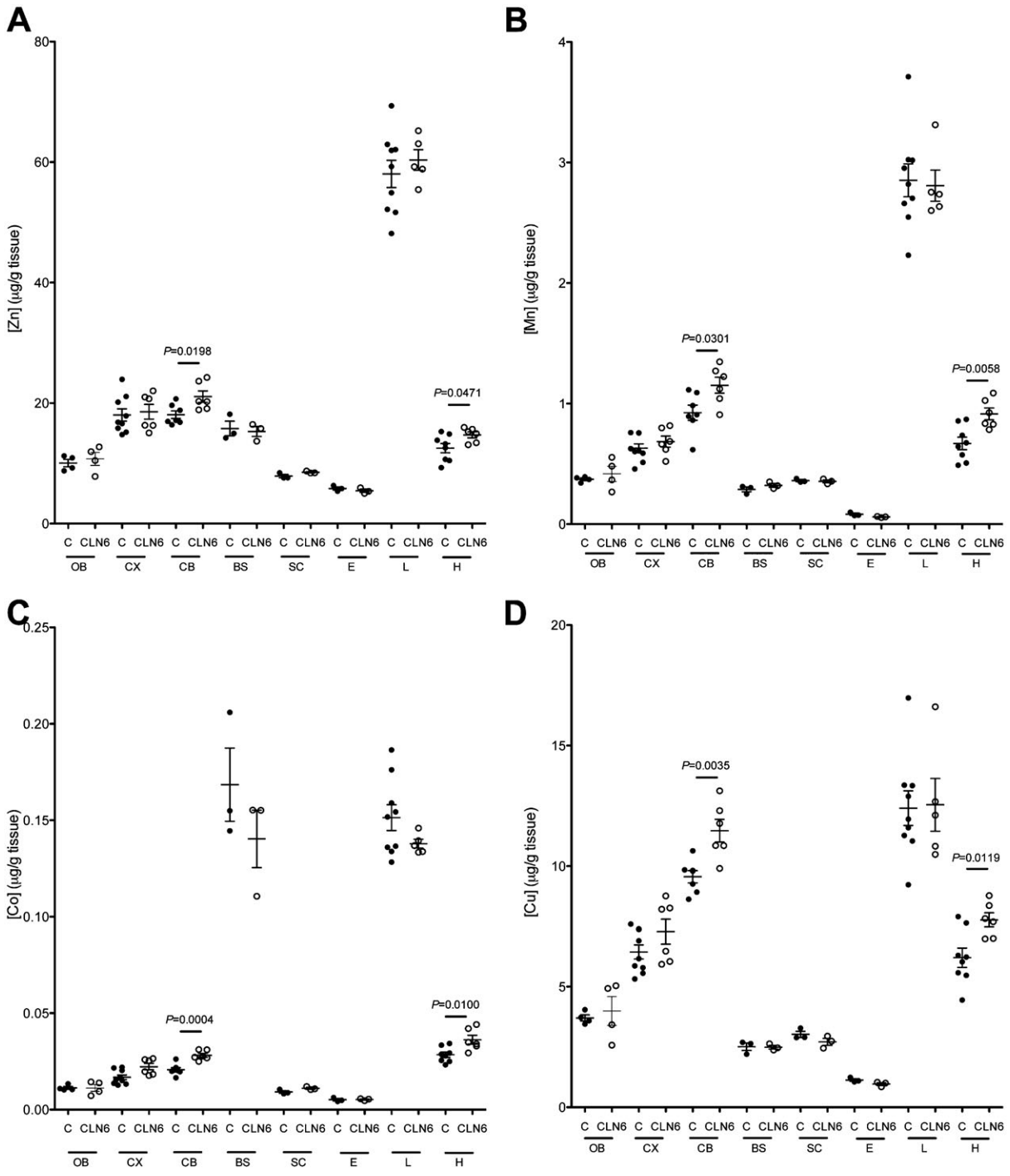

Fig. 4. Biometals accumulate in the cerebellum and heart of 24 week old CLN6 mice. Metal concentrations in the CNS and peripheral tissues of 24 week old control and mutant CLN6 mice were measured using ICP-MS. The concentrations of zinc (**A**), manganese (**B**), cobalt (**C**) and copper (**D**) in each tissue are expressed as mean±S.D. values. C, control; OB, olfactory bulb; CX, cortex; CB, cerebellum; BS, brainstem; SC, spinal cord; E, eye; L, liver; H, heart. *P* values determined by Student's *t* test.

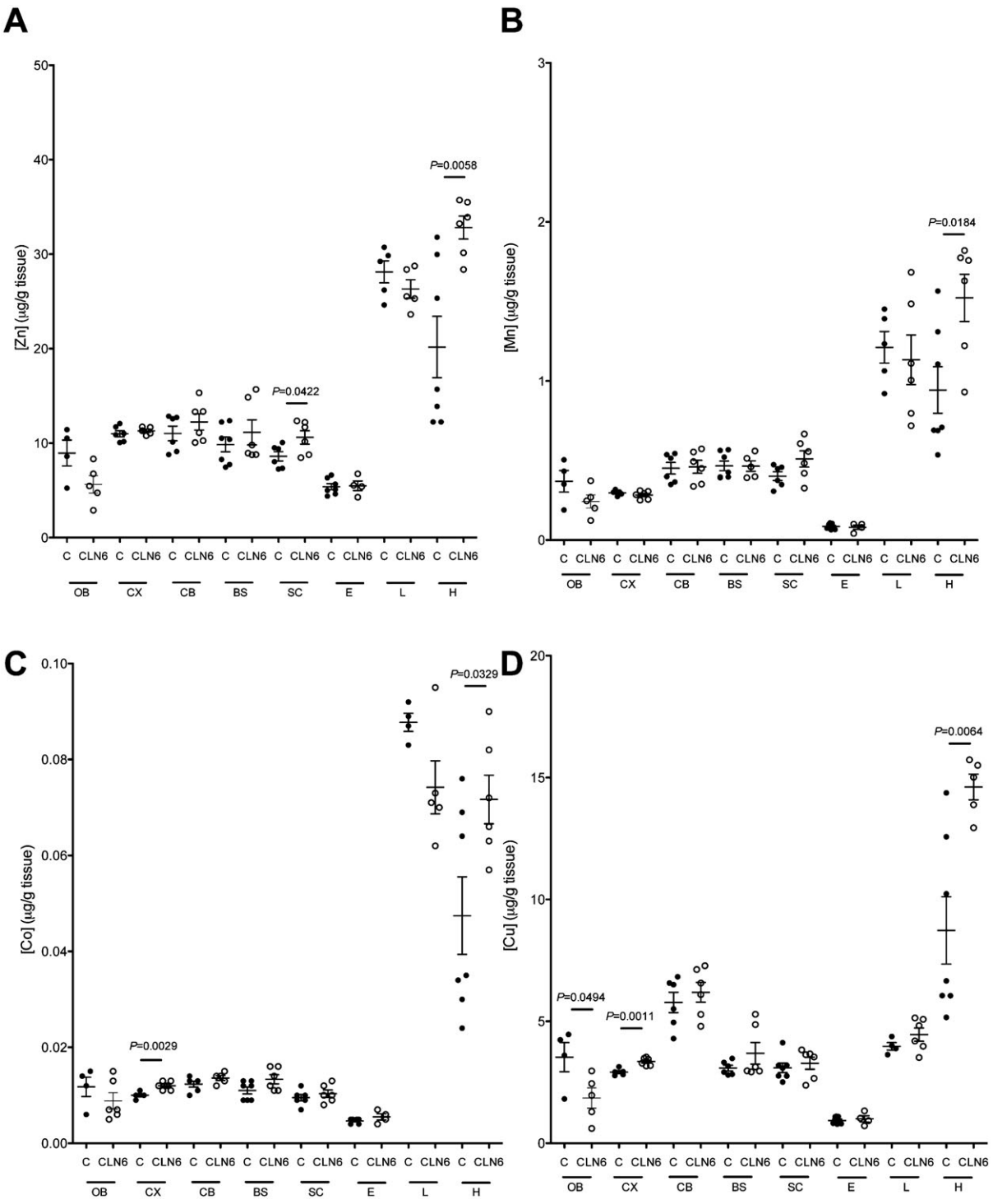

Fig. 5. Biometal changes in the cortex, spinal cord, olfactory bulb and heart in 32 week old CLN6 mice. Metal concentrations in the CNS and peripheral tissues of 32 week old control and mutant CLN6 mice were measured using ICP-MS. The concentrations of zinc (**A**), manganese (**B**), cobalt (**C**) and copper (**D**) in each tissue are expressed as mean±S.D. values. C, control; OB, olfactory bulb; CX, cortex; CB, cerebellum; BS, brainstem; SC, spinal cord; E, eye; L, liver; H, heart. *P* values determined by Student's *t* test.

Kinase levels are not altered in CLN6 mice

Functional outcomes of metal dyshomeostasis may involve the perturbation of normal cell signaling mechanisms. Biometal accumulation has been reported to induce aberrant activation of the Akt/glycogen synthase kinase 3 (GSK3) and extracellular signal-regulated kinase 1/2 (ERK) cellular signaling cascades (Min et al., 2007; He and Aizenman, 2010). We previously demonstrated sustained activation of cellular kinase pathways in an ovine model of CLN6 disease (Kanninen et al., 2013). We therefore employed western immunoblotting to determine

whether biometal accumulation in CLN6 brain regions was associated with alterations to the phosphorylated forms of Akt/GSK3 or ERK. The 24-week old age group was selected for these analyses as the most pronounced and consistent presymptomatic changes in both CLN6 mRNA expression and metal accumulation were detected in the cerebellum at this age. We detected no significant differences in global Akt, GSK3 or ERK phosphorylation in the olfactory bulb, cortex or cerebellum of 24 week old control and CLN6 mice (supplementary material Fig. S2A–L). To assess localized differences in kinase activation profiles, we performed immunofluorescence on P-GSK3 and P-ERK-stained coronal sections from the cerebellum and motor cortex of control and CLN6 mice. However, no differences to kinase phosphorylation states were observed (data not shown). Taken together, these data indicate that localized biometal transporter changes can occur independently of substantially altered cellular kinase activity. However, whether rapid, transient changes in kinase activity are associated with altered biometal homeostasis is unknown.

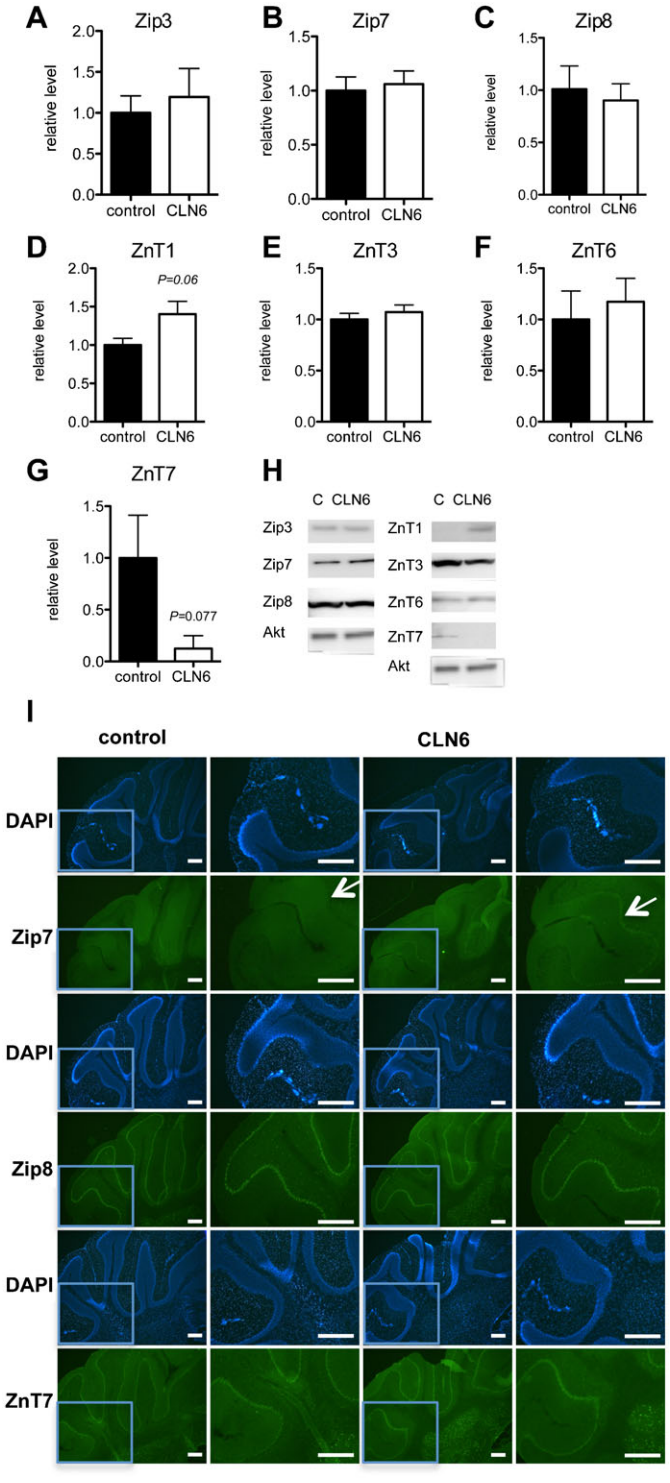

Localized alterations to metal transport proteins in CLN6 affected brains

Intracellular distribution of zinc, manganese and additional biometals is largely controlled in mammalian cells by cation transport proteins, primarily the Zip/SLC39A and ZnT/SLC30A family members (for reviews, see Sekler et al., 2007; Dempski, 2012) as well as P-type ATPases (ATP7A/B and ATP13A2). Zip/SLC39A family proteins increase cytoplasmic metal concentrations by regulating the influx of biometals into the cytoplasm, whereas ZnT/SLC30A family members mediate biometal efflux into cellular organelles or the extracellular space. To investigate whether the observed biometal accumulation was associated with alterations to the global levels of metal transporters, we performed western immunoblotting on CLN6 and control mouse cerebella. This was compared to cerebral cortex as global metal concentrations were not altered in this brain region of the CLN6 mice at this age.

Metal transporter levels were not significantly altered in the CLN6 mouse whole cerebella homogenates, although we detected a trend towards increased ZnT1 and decreased ZnT7 levels (Fig. 6A–H). Similarly, metal transporter levels were unchanged in the cortex of CLN6 animals (supplementary material Fig. S3A–I). We hypothesised that localized changes to metal transporter expression in a sub-population of neuronal or glial cells may be masked by the lack of global changes to metal transporter protein levels and hence, performed immunofluorescent staining on fixed coronal cerebellar sections from control and CLN6 animals with antibodies directed against several metal transporters. Although the most pronounced alteration to metal transport levels in the cerebella homogenates were observed in ZnT7, examination of the localized cerebellar ZnT7 distribution revealed no obvious differences between control and CLN6 animals (Fig. 6I). Similarly, no differences were observed in cerebellar Zip8 staining (Fig. 6I). Conversely, there were striking differences in the cerebellar distribution of the ER/Golgi-resident metal transporter, Zip7 (Taylor et al., 2004; Huang et al., 2005). Indeed, the Purkinje cell layer, which was

Fig. 6. Zip7 transporter distribution is altered in the cerebellar Purkinje cell layer of pre-symptomatic CLN6 mice. (**A–G**) Cerebellar homogenates (5–30 µg) isolated from 24-week old control or CLN6 mice (n=3 per group) were immunoblotted with antibodies directed against members of the Zip (SLC39A) or ZnT (SLC30A) families of metal transporters. GAPDH, β-tubulin, total Akt or total ERK, as appropriate, were used as loading controls. Densitometry quantification was performed in ImageJ and metal transporter levels are expressed relative to those in control mice. (**H**) Representative immunoblots demonstrating metal transporter levels in cerebellum. (**I**) Immunofluorescent staining of coronal cerebellar sections (Bregma −5.8 mm) from 24 week-old control and CLN6 mice was used to assess localized variations in Zip7, Zip8 and ZnT7 expression. Arrows indicate Purkinje cells. Nuclei were stained blue with DAPI. Images are representative of 3 mice per genotype. Scale bars: 100 µm.

reported to be the site of significant lipofuscin accumulation in 52 week old CLN6 mice (Thelen et al., 2012b), revealed substantially stronger immunopositive labeling of Zip7 protein in CLN6 as compared to control animals (Fig. 6I). Interestingly, these changes were site-specific, as they were not observed in the motor cortex of CLN6 animals (supplementary material Fig. S3). As the heart was a site of significant biometal accumulation, we investigated whether localized biometal transporter changes could be detected. However, apparent morphological differences between control and CLN6 heart tissue prevented accurate determination of expression differences (data not shown). We are further investigating the basis of these changes. Our findings indicate that cerebellar biometal accumulation in 24-week old CLN6 mice is accompanied by localized upregulation of Zip7, specifically in cells that later reveal key neuropathological changes in this model.

Zip7 changes are associated with biometal redistribution in presymptomatic CLN6 mouse brain

Finally, we examined whether significant changes occurred to biometal re-distribution at a sub-cellular level as such changes may not be detected by ICP-MS analysis of brain homogenates. To investigate this, we performed sucrose density gradient centrifugation of whole mouse brains collected from 24 week old control and CLN6 littermates and analysed fractions for metal content by ICP-MS. Whole brains were required to facilitate biometal detection at a sub-cellular level. To match fractions with corresponding organelles, western blotting using antibodies to cellular organelle markers was performed. The ratio of zinc in CLN6 compared to control brain fractions was up to 3 fold greater in the fractions that were positive for the ER markers PDI and calnexin (Fig. 7A). Cobalt and manganese concentrations were also elevated in the ER fractions of CLN6 brains (Fig. 7B, C). Zinc, copper and cobalt were elevated in the CLN6 brain fractions containing the lysosomal marker, lysozyme, the early endosome marker, Rab5, and the Golgi marker, Golgi 97 (Fig. 7A,B,D). We examined the expression of Zip7 in these fractions, and determined that Zip7 was elevated in CLN6 brains in fractions 3–12, which corresponded to lysosomes, endosomes and Golgi (Fig. 7E). CLN6 expression in fractions was below detectable limits by western blotting (data not shown). Together, these data indicate that there are complex changes to sub-cellular biometal distribution and metal transporter metabolism in CLN6 mouse brain and that specific biometals potentially accumulate in several different organelles.

Discussion

This study characterized the behavioural phenotype of CLN6 mice and demonstrated that regional CLN6 transcript loss is associated with accumulation of a number of biologically important metals. Decreased CLN6 expression was accompanied by localized changes to a cellular biometal transporter, Zip7, specifically in Purkinje cells, and in sub-cellular fractions of whole brain homogenates.

CLN6 mice display progressive motor and visual symptoms

Although it is accepted that CLN6 mice are phenotypically normal until 8 months of age, this study represents the first rigorous behavioural analysis of CLN6 mice throughout disease progression. We observed progressive motor and visual decline from the ages of 34 and 42 weeks, respectively. Motor symptoms were detected earliest by the accelerating rotarod test, indicating that rotarod performance is the most effective behavioural measure allowing early discrimination between control and CLN6 mice.

Spatio-temporal loss of CLN6 mRNA predicts biometal accumulation

To gain a better understanding of physiological CLN6 expression patterns in health and disease and provide a clue to the function of CLN6, we performed a spatio-temporal analysis of CLN6 mRNA expression levels. As impaired biometal homeostasis is a hallmark of neurodegeneration (Barnham et al., 2004), and we previously demonstrated altered biometal concentrations in CLN6 Merino and South Hampshire sheep (Kanninen et al., 2013), the relationship between biometal homeostasis and CLN6

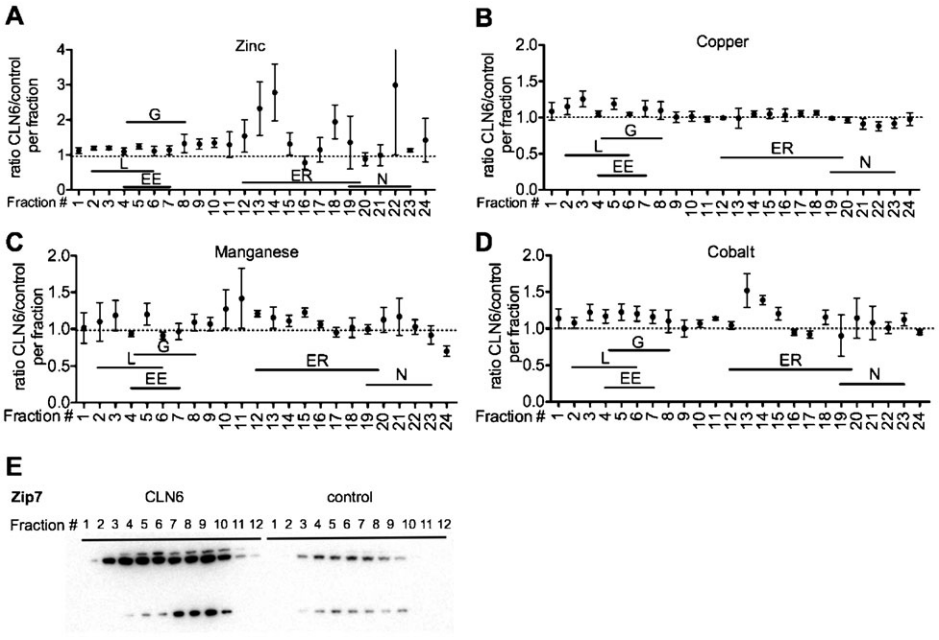

Fig. 7. Biometals accumulate in lysosomes and ER in presymptomatic CLN6 mouse brain. Sucrose density gradient fractions from 24 week old whole mouse brain were analysed for metal content by ICP-MS. Data are expressed as the mean±S.D of the ratio of zinc (**A**), manganese (**B**), cobalt (**C**) and copper (**D**) concentrations in CLN6 brains relative to control brains from 3 independent experiments. Dotted lines represent equal metal content in control and CLN6 brains. Organelles corresponding to fraction numbers are based on western blotting analyses. L, lysosomes; EE, early endosomes; ER, endoplasmic reticulum; G, Golgi apparatus; N, nucleus. (**E**) Representative immunoblot of Zip7 protein present in control and CLN6 fractions.

mRNA expression was also assessed. Here we demonstrate accumulation of the same biometals, demonstrating that specific biometal imbalances occur in multiple models of CLN6 disease.

We observed an inverse association between CLN6 expression levels and biometal concentrations in presymptomatic CLN6 mice. Specifically, at 12 weeks of age, the most pronounced alterations to the levels of both CLN6 transcripts and tissue biometals were observed in the spinal cord and heart, whereas at 24 weeks of age, both CLN6 transcript and biometal changes were detected in the cerebellum and heart. Nonetheless, loss of CLN6 expression alone was not predictive of substantial biometal change, as the dramatic reduction in CLN6 expression in the eye of presymptomatic CLN6 mice was not accompanied by biometal changes. A minimum threshold of CLN6 expression level may be sufficient to maintain biometal homeostasis, while loss of CLN6 transcripts below the threshold may promote biometal accumulation. Indeed, the tissues with the lowest CLN6 mRNA expression were the cerebellum, olfactory bulb and heart at all ages, and the spinal cord of CLN6 mice at 12 weeks of age (Fig. 2). Interestingly, biometal accumulation occurs in these tissues, specifically when significant loss of CLN6 transcript is detected in each respective tissue. That different tissues are affected at different stages of disease may reflect progression of pathology throughout different brain regions.

These data provide the first link between CLN6 expression and biometal homeostasis in CLN6 disease. Biometals are tightly regulated within the CNS with very little variation and even the small changes observed here may have important biological consequences (Malm et al., 2007). Moreover, due to progressive disease changes, a linear change in metals is unlikely to occur, instead, the complex pattern of changes observed reflects the complex nature of metal homeostasis across the disease. Importantly, biometal imbalances occur early in this model and are associated with presymptomatic CLN6 expression, indicating that biometal homeostasis is likely to contribute to pathology rather than occur concomitantly with disease symptoms.

The heart is a site of sustained biometal accumulation and CLN6 transcript loss

CLN6 expression was reduced in the heart at all time points, which occurred concomitantly with sustained biometal accumulation. Moreover, at 32 weeks, zinc, manganese, copper, cobalt and magnesium all significantly accumulated in the heart, and the increases in each biometal were 60–75% over controls. Magnesium plays a key role in the cardiac electrical conduction systems and is required to maintain a regular heartbeat (reviewed by Fazekas et al., 1993), a phenotype that is impaired in NCLs. This suggests that retention of magnesium in CLN6 animals may be a compensatory mechanism to counteract the abnormalities in heart function. It is also noteworthy that lipopigment is consistently reported to accumulate in heart tissue, and cardiac abnormalities have been described in various NCL models and patients (Michielsen et al., 1984; Galvin et al., 2008; Ostergaard et al., 2011; Fukumura et al., 2012). However, this is the first study to implicate the heart as an important region in CLN6 disease and the first to provide presymptomatic evidence of significant cardiac changes in a model of NCL disease.

Zip7 is specifically altered in CLN6 Purkinje cells

To determine if biometal accumulation was a result of altered intracellular biometal trafficking, we investigated the regional levels of the Zip and ZnT proteins in presymptomatic CLN6 mice. Initially identified for their ability to transport zinc across membranes, Zip/ZnT transporters have recently been implicated in the transport of other transition metals, including those altered in CLN6 mice, with a similar efficiency to zinc (Pinilla-Tenas et al., 2011; Antala and Dempski, 2012; Nam and Knutson, 2012; Wang et al., 2012).

We observed localized changes to the levels of Zip7, an ER and Golgi-resident transmembrane cation transporter that controls import of biometals from the ER/Golgi to the cytoplasm (Taylor et al., 2004; Huang et al., 2005), specifically in those tissues that reveal neuropathological changes. Indeed, the cerebellar Purkinje layer, which revealed strong Zip7 protein expression in CLN6 but not control brains (Fig. 6I), is a site of significant lipopigment accumulation at 52 weeks of age in CLN6 mice (Thelen et al., 2012b). Moreover, Purkinje cell loss was reported to be an early pathological feature in mouse models of infantile, late infantile and juvenile NCL diseases (Sleat et al., 2004; Macauley et al., 2009; Weimer et al., 2009), and oral treatment of rats with manganese for 30 days resulted in cerebellar Purkinje cell loss and morphological abnormalities (Chtourou et al., 2012). Importantly, Purkinje cells are essential for controlling motor and learning functions, and motor symptoms were the first to be detected in this model (Fig. 1C). Consistent with previous reports, Zip7 was detected in whole murine brain fractions containing the Golgi marker, Golgi 97 (Huang et al., 2005). While differences in Zip7 expression between control and CLN6 animals were not detected in cerebellar or cortical homogenates, using a more sensitive approach, we observed elevated Zip7 in fractions isolated from whole fresh brains of CLN6 animals. Additionally, we detected specific accumulation of zinc, copper, cobalt and manganese in the fractions containing ER, Golgi and lysosomal components. Given the ER/Golgi localization of both CLN6 and Zip7, and in light of the substantial Zip7 expression changes in Purkinje cells, we hypothesize that CLN6 and Zip7 may directly interact. Mutation of CLN6 may result in altered interactions, thereby promoting biometal accumulation in subcellular compartments in CLN6 mice.

It is possible that the mutant CLN6 protein may have impaired function or be prematurely cleared. Nonetheless, investigating the spatio-temporal transcription levels of CLN6 in health and disease may provide clues regarding its physiological function. The CLN6 expression patterns observed in this study contrast earlier findings, where CLN6 mRNA expression was greatest in cerebellum, especially in Purkinje layer (Thelen et al., 2012a). The difference can be attributed to the different ages of mice used, as that study examined CLN6 mRNA levels in 28 day old (4 week old) mice, whereas the mice in the present study were between 12 and 32 weeks of age. While high expression of CLN6 transcripts in young mice suggests a developmental role of CLN6, our results indicate that CLN6 may have additional roles in regulation of biometal homeostasis in adult neuronal cells.

We also investigated the role of the signaling kinases, Akt, GSK3, and ERK, that were reported to be biometal-regulated (Min et al., 2007; He and Aizenman, 2010). The Akt/GSK3 and ERK pathways are normally transiently activated in response to specific extracellular signals, but are commonly deregulated in the context of disease, particularly in neurodegeneration (Colucci-D'Amato et al., 2003) and were chronically phosphorylated in the brains of CLN6 sheep. Curiously, we observed no significant changes to the Akt/GSK3 or ERK pathways in the brains of CLN6 mice. However, a lack of permanent kinase activation does not necessarily preclude the

involvement of aberrant Akt/GSK3 or ERK signaling in CLN6 disease, as subcellular signaling cascades are controlled by a series of rapid and transient phosphorylation and dephosphorylation events that may have been missed by analysis of steady-state levels of phosphorylated kinases.

Despite the recognized role of impaired biometal homeostasis in the pathology of a number of neurodegenerative disorders (Barnham et al., 2004; Bolognin et al., 2009), and the commonalities in pathology between NCLs and other forms of neurodegeneration (reviewed by Jalanko and Braulke, 2009), the role of biometals in NCLs has not been directly explored. However, some evidence exists to suggest that biometal homeostasis may be altered in NCLs. Reports have found that metal supplementation affected CLN7 gene expression (Johnstone and Milward, 2010), changes in metal transporter ZnT6 expression in CLN6 and CLN3 cell lines (Cao et al., 2011), and interactions between CLN3 and a sodium–potassium pump (Uusi-Rauva et al., 2008). Moreover, mutations in the lysosomal biometal transporter ATP13a2 (Medici et al., 2012) can result in Parkinsonism or NCL-associated neurodegeneration depending on the site of mutation (Ramirez et al., 2006; Bras et al., 2012). Our findings here demonstrate that an additional zinc/manganese transporter, Zip7, may be involved in neurodegenerative changes. Moreover, our brain fractionation studies indicated that Zip7 expression may also be altered in CLN6 lysosomes. Our study provides the first direct examination of biometal homeostasis in any childhood neurodegenerative disorder. Future studies will investigate how the loss of CLN6 may trigger changes in Zip7, and how this results in cellular biometal redistribution. Moreover, investigation of biometal levels in other NCL models is currently underway in our laboratory, to determine whether impaired metal homeostasis is a feature common to multiple NCL forms.

Materials and Methods

Mice

Animal handling and experimentation were performed in accordance with national and institutional (The University of Melbourne) guidelines (AEC no. 1112024). The genotype of affected CLN6 (B6.Cg-*Cln6nclf*/J mice, The Jackson Laboratory (Bronson et al., 1998)) mice was determined using TaqMan SNP genotyping assays (Life Technologies). Unaffected littermates that were homozygous for wild-type CLN6 (C57BL/6J) were used as controls. Brain samples (minimum $n=5$ per group) were collected from mice of either sex at 12, 24, 32 weeks of age and at disease end stage. In accordance with ethical guidelines, the criteria for end stage included full hind limb paralysis, over 15% weight loss from peak body weight or rotarod performance less than 10 seconds in 2 consecutive trials. Mice were weighed twice-weekly.

Mice were killed by an intraperitoneal injection of 2 mg/g ketamine (Lyppard Australia) and 400 µg/g xylazine (Lyppard Australia) and were transcardially perfused with 0.9% (w/v) saline containing 0.01% (w/v) heparin. At post mortem, whole brains were stored in 4% paraformaldehyde (PFA) solution or dissected into the following regions: olfactory bulb, cortex, cerebellum and brain stem, and immediately frozen in liquid nitrogen. The spinal cord, eye, liver and heart were also collected and frozen for biochemical and metal analyses.

Accelerating rotarod

The rotarod apparatus (AccuScan Instruments, Columbus, Ohio) was used to monitor disease progression, motor function and balance of CLN6 mice and control littermates ($n=22$-24 per genotype). Mice were trained on the rotarod for 3 consecutive days before the start of the trial. Beginning at the age of 14 weeks, mice were tested once a week. The rotarod began at 4 rpm and accelerated to 40 rpm over 180 seconds. The latency to fall off was recorded. Each mouse participated in two trials and the best result of each session was used for statistical analyses.

Inverted grid test of grip strength

The grip strength of the mice was tested weekly beginning at the age of 14 weeks. Mice were placed on a standard cage lid prior to carefully rotating the lid 180° at a height of approximately 30 cm above a soft surface (Brooks et al., 2012; Heuer et al., 2012). The duration the mouse spent grasping the grid without falling was recorded with a maximum of 180 seconds. Each week the mice underwent 2 trials and the best result of the two trials was used for statistical analyses.

Vision test

The visual placing response was tested to assess the function of the visual system (Metz and Schwab, 2004) once a week. As the mouse was suspended by the tail and lowered towards a bench, the mouse extended its forelimbs to place them onto the surface. The mean response was rated in two trials with the following scoring system: 0 indicates no placing response, 1 indicates a weak placing response and 2 indicates a clear placing response.

Metal analyses

The metal content in 5 regions of the mouse CNS and 3 peripheral mouse tissues was measured using inductively coupled plasma mass-spectrometry (ICP-MS) as previously described (Price et al., 2011). Briefly, weighed tissue pieces were lyophilized, digested in nitric acid overnight, and heated at 90℃ for 20 minutes. The acid treated samples were then treated with hydrogen peroxide. After 30 minutes, the samples were heated for a further 15 minutes at 70℃. All samples were diluted in 1% nitric acid before being measured using an Agilent 7700 series ICP-MS instrument using a Helium Reaction Gas Cell. The instrument was calibrated using 0, 5, 10, 50, and 100 ppb of certified multi-element ICP-MS standard calibration solutions (Accustandard) for a range of elements. Concentrations of the following elements were assessed: ^{7}Li, ^{11}B, ^{23}Na, ^{24}Mg, ^{27}Al, ^{31}P, ^{39}K, ^{43}Ca, ^{47}Ti, ^{52}Cr, ^{55}Mn, ^{56}Fe, ^{59}Co, ^{60}Ni, ^{63}Cu, ^{66}Zn, ^{69}Ga, ^{72}Ge, ^{78}Se, ^{85}Rb, ^{88}Sr, ^{95}Mo, ^{101}Ru, ^{111}Cd, ^{118}Sn, ^{137}Ba, ^{182}W, ^{208}Pb. The following metals were below the limit of detection: ^{7}Li, ^{11}B, ^{47}Ti, ^{52}Cr, ^{60}Ni, ^{69}Ga, ^{72}Ge, ^{78}Se, ^{85}Rb, ^{95}Mo, ^{111}Cd, ^{137}Ba, ^{182}W, ^{208}Pb. 200 ppb of Yttrium (Y89) was used as an internal control (Accustandard). The results are expressed as micrograms of metal per gram of wet weight (µg/g).

RNA isolation and cDNA preparation

RNA was prepared from snap frozen mouse specimens (10 mg) using the MagMax™ Total RNA isolation kit (Life Technologies) according to manufacturer's instructions. RNA concentrations were measured using the Qubit® 2.0 fluorometer (Life Technologies). RNA (200 ng) was reverse transcribed using random hexamers and High Capacity cDNA kit (Life Technologies).

qRT-PCR

TaqMan Gene Expression assays for CLN6 and β-tubulin alpha3a were purchased from Life Technologies (Mm01179411_m1 and Mm00833707_mH, respectively) and performed according to manufacturer's instructions. Each reaction mix contained 0.5 µl of Taqman Gene Expression assays containing FAM-labelled probes, 5 µl of 2× TaqMan Fast Advance Gene Expression Master mix and 4 µl of cDNA template (synthesized from 10 ng RNA per reaction). Duplicate reactions were performed using the LightCycler 480 (Roche) using conditions recommended by the manufacturer. Cycle threshold (Ct) values were calculated as the lowest cycle number producing an exponential increase in PCR product amplification. Delta Ct method was used for normalization of expression relative to β-tubulin.

Western blots

Brain and heart tissues were homogenized with a Dounce tissue grinder in Phosphosafe extraction reagent (Novagen) containing protease inhibitor cocktail (Roche) and DNAse (Roche). The protein concentrations of supernatants after centrifugation (12,000×*g*, 5 minutes, 4℃) were measured with BCA assay kit (Pierce) according to manufacturer's instructions. Equal protein amounts were separated on 12% SDS-PAGE Tris-glycine gels. Proteins were transferred to PVDF membranes and blocked with 4% skim milk solution in PBS-Tween. Membranes were probed overnight with primary antibodies diluted in 4% skim milk solution in PBS-Tween. Unless stated otherwise, primary antibodies were diluted 1:1000. Antibodies were directed against: Zip3 (Abnova), Zip7 (1:2000, Proteintech), Zip8 (1:1200, Proteintech), Zip14 (Novus), ZnT1 (Sigma), ZnT3 (Proteintech), ZnT6 (1:1200, Proteintech), ZnT7 (Proteintech), as well as the phosphorylated forms of the proteins ERK1/2, Akt and GSK-3 (Cell Signaling Technologies). Antibodies for organelle markers included: PDI (Enzo Biochem), calnexin (Abcam), Rab5 (Abcam), lysozyme (Abcam), histone H3 (Cell Signaling Technologies). The horseradish peroxidase-conjugated anti-rabbit secondary antibodies (Cell Signaling Technologies) were used at a dilution of 1:5000. Membranes were developed by chemiluminescence (Amersham ECL Advance Western blotting detection kit) and imaged on a Fujifilm LAS3000 Imager (Berthold). Western blots were subjected to densitometry analysis using ImageJ software. Target band intensity was compared to the intensity of control bands using blots probed with antibodies directed against the control proteins, GAPDH and total Akt. Relative protein levels in CLN6 animals were determined by normalization to the levels in control animals.

Sucrose density gradient fractionation

Whole brains were removed from 24 week old control and CLN6 littermates that had been killed by cervical dislocation and subjected to sucrose density centrifugation. Briefly, brains were washed in PBS containing 0.25 M sucrose and homogenized using a Dounce Homogenizer in 1 mL of homogenization buffer (containing 300 mM sucrose, 5 mM EDTA, 5 mM HEPES, 1 µM phenylmethanesulfonylfluoride (PMSF) and protease inhibitors, pH 7.4). Homogenates were aspirated through a 25G needle 10 times and centrifuged (10,000×*g*, 10 minutes, 4℃). Supernatant concentrations were standardized in sucrose gradient buffer (containing 150 mM NaCl, 10 mM HEPES, 1 mM EDTA, 100 µM $MgCl_2$ and protease inhibitors, pH 7.4). Samples were applied to sucrose gradients, constructed by layering 10–40% w/v sucrose in centrifuge tubes (Beckman), and centrifuged at 100,000×*g* for 16 hours in a Beckman Ultracentrifuge (SW41Ti rotor). Twenty four 500 µL fractions were collected and stored at −20℃ prior to analysis by Western blot or ICP-MS.

Immunofluorescent staining

Whole mouse brains (n=3 per genotype) were fixed in 4% PFA at 4℃ for 21 hours. Brains were cryoprotected in 30% sucrose solution in PBS for 48 hours at 4℃ then frozen in liquid nitrogen. Serial coronal brain sections (5 µm thick) were cut using a cryostat from the brains of 24 week-old control and CLN6 mice. Sections corresponding to the regions containing cerebellum (Bregma −5.8 mm) and motor cortex (Bregma 1.70 mm) were analysed using immunofluorescence. Sections were washed twice in phosphate buffered saline (PBS), washed twice in PBS containing 0.05% (v/v) Tween 20, then permeabilized for 5 minutes in 0.2% (v/v) Triton X-100. After three PBS-Tween washes, sections were blocked in 20% (v/v) normal goat serum in PBS, and incubated overnight with rabbit antibodies directed against Zip7 (1:2000), Zip8 (1:100) or ZnT7 (1:100) diluted in 20% (v/v) normal goat serum in PBS. Following a further three washes, immunocomplexes were detected with secondary Alexa-Fluor 488 conjugated goat-anti-rabbit antibodies, diluted 1:300 in 20% (v/v) normal goat serum in PBS. Cell nuclei were visualized with DAPI (1:10,000; Life Technologies). Coverslips were mounted onto microscope slides with fluorescence mounting media (DAKO).

Statistical analyses

Differences in survival were examined using the Log-rank (Mantel–Cox) Test (GraphPad Prism, version 5 software). The effects of genotypes on weight, rotarod performance, vision and grip strength were determined using 2-way ANOVA in GraphPad Prism software. Post-hoc Bonferonni tests were used to determine the age at which means became significantly different between genotypes. Differences in metal content, CLN6 mRNA expression and protein levels were determined using unpaired Student's *t*-tests. *P* values below 0.05 were considered significant. Data are expressed as mean±S.D.

Acknowledgements

We thank Nastasia Lim for her help with the mouse behavioural testing. This work was supported by The Sigrid Juselius Foundation [grant number 1512032 to K.M.K]; the Academy of Finland [grant number 135625 to K.M.K]; the Australian Research Council (ARC) [DP110101368]; and National Health and Medical Research Council of Australia (NHMRC) [628946]. A.R.W. is a recipient of an ARC Future Fellowship [FT100100674]. The funding sources had no influence in study design; in the collection, analysis and interpretation of data; in the writing of the report; and in the decision to submit the article for publication.

Author Contributions

A.G., A.R.W. and K.M.K. designed experiments. A.G., K.M.K., C.D., S.J.P., A.C., G.E.L., I.V. and G.G. performed research. A.G., I.V., A.R.W. and K.M.K. analyzed the data. A.G. and K.M.K. wrote the paper. A.R.W. and P.J.C. provided critical revisions of the manuscript.

Competing Interests

The authors have no competing interests to declare.

References

Antala, S. and Dempski, R. E. (2012). The human ZIP4 transporter has two distinct binding affinities and mediates transport of multiple transition metals. *Biochemistry* **51**, 963-973.

Barnham, K. J., Masters, C. L. and Bush, A. I. (2004). Neurodegenerative diseases and oxidative stress. *Nat. Rev. Drug Discov.* **3**, 205-214.

Beyer, N., Coulson, D. T., Heggarty, S., Ravid, R., Hellemans, J., Irvine, G. B. and Johnston, J. A. (2012). Zinc transporter mRNA levels in Alzheimer's disease postmortem brain. *J. Alzheimers Dis.* **29**, 863-873.

Bolognin, S., Messori, L. and Zatta, P. (2009). Metal ion physiopathology in neurodegenerative disorders. *Neuromolecular Med.* **11**, 223-238.

Bras, J., Verloes, A., Schneider, S. A., Mole, S. E. and Guerreiro, R. J. (2012). Mutation of the parkinsonism gene ATP13A2 causes neuronal ceroid-lipofuscinosis. *Hum. Mol. Genet.* **21**, 2646-2650.

Bronson, R. T., Donahue, L. R., Johnson, K. R., Tanner, A., Lane, P. W. and Faust, J. R. (1998). Neuronal ceroid lipofuscinosis (nclf), a new disorder of the mouse linked to chromosome 9. *Am. J. Med. Genet.* **77**, 289-297.

Brooks, S., Higgs, G., Jones, L. and Dunnett, S. B. (2012). Longitudinal analysis of the behavioural phenotype in Hdh(CAG)150 Huntington's disease knock-in mice. *Brain Res. Bull.* **88**, 182-188.

Cao, Y., Staropoli, J. F., Biswas, S., Espinola, J. A., MacDonald, M. E., Lee, J. M. and Cotman, S. L. (2011). Distinct early molecular responses to mutations causing vLINCL and JNCL presage ATP synthase subunit C accumulation in cerebellar cells. *PLoS ONE* **6**, e17118.

Chtourou, Y., Fetoui, H., Garoui, E. M., Boudawara, T. and Zeghal, N. (2012). Improvement of cerebellum redox states and cholinergic functions contribute to the beneficial effects of silymarin against manganese-induced neurotoxicity. *Neurochem. Res.* **37**, 469-479.

Colucci-D'Amato, L., Perrone-Capano, C. and di Porzio, U. (2003). Chronic activation of ERK and neurodegenerative diseases. *Bioessays* **25**, 1085-1095.

Dempski, R. E. (2012). The cation selectivity of the ZIP transporters. *Curr Top Membr* **69**, 221-245.

Fazekas, T., Scherlag, B. J., Vos, M., Wellens, H. J. and Lazzara, R. (1993). Magnesium and the heart: antiarrhythmic therapy with magnesium. *Clin. Cardiol.* **16**, 768-774.

Fukumura, S., Saito, Y., Saito, T., Komaki, H., Nakagawa, E., Sugai, K., Sasaki, M., Oka, A. and Takamisawa, I. (2012). Progressive conduction defects and cardiac death in late infantile neuronal ceroid lipofuscinosis. *Dev. Med. Child Neurol.* **54**, 663-666.

Galvin, N., Vogler, C., Levy, B., Kovacs, A., Griffey, M. and Sands, M. S. (2008). A murine model of infantile neuronal ceroid lipofuscinosis-ultrastructural evaluation of storage in the central nervous system and viscera. *Pediatr. Dev. Pathol.* **11**, 185-192.

Gao, H., Boustany, R. M., Espinola, J. A., Cotman, S. L., Srinidhi, L., Antonellis, K. A., Gillis, T., Qin, X., Liu, S., Donahue, L. R. et al. (2002). Mutations in a novel CLN6-encoded transmembrane protein cause variant neuronal ceroid lipofuscinosis in man and mouse. *Am. J. Hum. Genet.* **70**, 324-335.

He, K. and Aizenman, E. (2010). ERK signaling leads to mitochondrial dysfunction in extracellular zinc-induced neurotoxicity. *J. Neurochem.* **114**, 452-461.

Heuer, A., Smith, G. A., Lelos, M. J., Lane, E. L. and Dunnett, S. B. (2012). Unilateral nigrostriatal 6-hydroxydopamine lesions in mice I: motor impairments identify extent of dopamine depletion at three different lesion sites. *Behav. Brain Res.* **228**, 30-43.

Huang, L., Kirschke, C. P., Zhang, Y. and Yu, Y. Y. (2005). The ZIP7 gene (Slc39a7) encodes a zinc transporter involved in zinc homeostasis of the Golgi apparatus. *J. Biol. Chem.* **280**, 15456-15463.

Jalanko, A. and Braulke, T. (2009). Neuronal ceroid lipofuscinoses. *Biochim. Biophys. Acta* **1793**, 697-709.

Johnstone, D. and Milward, E. A. (2010). Genome-wide microarray analysis of brain gene expression in mice on a short-term high iron diet. *Neurochem. Int.* **56**, 856-863.

Kanninen, K. M., Grubman, A., Meyerowitz, J., Duncan, C., Tan, J. L., Parker, S. J., Crouch, P. J., Paterson, B. M., Hickey, J. L., Donnelly, P. S. et al. (2013). Increased zinc and manganese in parallel with neurodegeneration, synaptic protein changes and activation of Akt/GSK3 signaling in ovine CLN6 neuronal ceroid lipofuscinosis. *PLoS ONE* **8**, e58644.

Kiselyov, K., Colletti, G. A., Terwilliger, A., Ketchum, K., Lyons, C. W., Quinn, J. and Muallem, S. (2011). TRPML: transporters of metals in lysosomes essential for cell survival? *Cell Calcium* **50**, 288-294.

Kousi, M., Lehesjoki, A. E. and Mole, S. E. (2012). Update of the mutation spectrum and clinical correlations of over 360 mutations in eight genes that underlie the neuronal ceroid lipofuscinoses. *Hum. Mutat.* **33**, 42-63.

Lovell, M. A., Smith, J. L., Xiong, S. and Markesbery, W. R. (2005). Alterations in zinc transporter protein-1 (ZnT-1) in the brain of subjects with mild cognitive impairment, early, and late-stage Alzheimer's disease. *Neurotox. Res.* **7**, 265-271.

Lyubartseva, G., Smith, J. L., Markesbery, W. R. and Lovell, M. A. (2010). Alterations of zinc transporter proteins ZnT-1, ZnT-4 and ZnT-6 in preclinical Alzheimer's disease brain. *Brain Pathol.* **20**, 343-350.

Macauley, S. L., Wozniak, D. F., Kielar, C., Tan, Y., Cooper, J. D. and Sands, M. S. (2009). Cerebellar pathology and motor deficits in the palmitoyl protein thioesterase 1-deficient mouse. *Exp. Neurol.* **217**, 124-135.

Malm, T. M., Iivonen, H., Goldsteins, G., Keksa-Goldsteine, V., Ahtoniemi, T., Kanninen, K., Salminen, A., Auriola, S., Van Groen, T., Tanila, H. et al. (2007). Pyrrolidine dithiocarbamate activates Akt and improves spatial learning in APP/PS1 mice without affecting beta-amyloid burden. *J. Neurosci.* **27**, 3712-3721.

Medici, S., Peana, M., Delogu, L. G. and Zoroddu, M. A. (2012). Mn(II) and Zn(II) interactions with peptide fragments from Parkinson's disease genes. *Dalton Trans.* **41**, 4378-4388.

Metz, G. A. and Schwab, M. E. (2004). Behavioral characterization in a comprehensive mouse test battery reveals motor and sensory impairments in growth-associated protein-43 null mutant mice. *Neuroscience* **129**, 563-574.

Michielsen, P., Martin, J. J., Vanagt, E., Vrints, C., Gillebert, T. and Snoeck, J. (1984). Cardiac involvement in juvenile ceroid lipofuscinosis of the Spielmeyer-Vogt-Sjögren type: prospective noninvasive findings in two siblings. *Eur. Neurol.* **23**, 166-172.

Min, Y. K., Lee, J. E. and Chung, K. C. (2007). Zinc induces cell death in immortalized embryonic hippocampal cells via activation of Akt-GSK-3beta signaling. *Exp. Cell Res.* **313**, 312-321.

Mole, S. E., Michaux, G., Codlin, S., Wheeler, R. B., Sharp, J. D. and Cutler, D. F. (2004). CLN6, which is associated with a lysosomal storage disease, is an endoplasmic reticulum protein. *Exp. Cell Res.* **298**, 399-406.

Nam, H. and Knutson, M. D. (2012). Effect of dietary iron deficiency and overload on the expression of ZIP metal-ion transporters in rat liver. *Biometals* **25**, 115-124.

Ostergaard, J. R., Rasmussen, T. B. and Mølgaard, H. (2011). Cardiac involvement in juvenile neuronal ceroid lipofuscinosis (Batten disease). *Neurology* **76**, 1245-1251.

Pinilla-Tenas, J. J., Sparkman, B. K., Shawki, A., Illing, A. C., Mitchell, C. J., Zhao, N., Liuzzi, J. P., Cousins, R. J., Knutson, M. D. and Mackenzie, B. (2011). Zip14 is a complex broad-scope metal-ion transporter whose functional properties support roles in the cellular uptake of zinc and nontransferrin-bound iron. *Am. J. Physiol.* **301**, C862-C871.

Price, K. A., Crouch, P. J., Volitakis, I., Paterson, B. M., Lim, S., Donnelly, P. S. and White, A. R. (2011). Mechanisms controlling the cellular accumulation of copper bis(thiosemicarbazonato) complexes. *Inorg. Chem.* **50**, 9594-9605.

Quadri, M., Federico, A., Zhao, T., Breedveld, G. J., Battisti, C., Delnooz, C., Severijnen, L. A., Di Toro Mammarella, L., Mignarri, A., Monti, L. et al. (2012). Mutations in SLC30A10 cause parkinsonism and dystonia with hypermanganesemia, polycythemia, and chronic liver disease. *Am. J. Hum. Genet.* **90**, 467-477.

Ramirez, A., Heimbach, A., Gründemann, J., Stiller, B., Hampshire, D., Cid, L. P., Goebel, I., Mubaidin, A. F., Wriekat, A. L., Roeper, J. et al. (2006). Hereditary parkinsonism with dementia is caused by mutations in ATP13A2, encoding a lysosomal type 5 P-type ATPase. *Nat. Genet.* **38**, 1184-1191.

Sekler, I., Sensi, S. L., Hershfinkel, M. and Silverman, W. F. (2007). Mechanism and regulation of cellular zinc transport. *Mol. Med.* **13**, 337-343.

Sharp, J. D., Wheeler, R. B., Lake, B. D., Savukoski, M., Järvelä, I. E., Peltonen, L., Gardiner, R. M. and Williams, R. E. (1997). Loci for classical and a variant late infantile neuronal ceroid lipofuscinosis map to chromosomes 11p15 and 15q21-23. *Hum. Mol. Genet.* **6**, 591-595.

Sleat, D. E., Wiseman, J. A., El-Banna, M., Kim, K. H., Mao, Q., Price, S., Macauley, S. L., Sidman, R. L., Shen, M. M., Zhao, Q. et al. (2004). A mouse model of classical late-infantile neuronal ceroid lipofuscinosis based on targeted disruption of the CLN2 gene results in a loss of tripeptidyl-peptidase I activity and progressive neurodegeneration. *J. Neurosci.* **24**, 9117-9126.

Sueta, C. A., Patterson, J. H. and Adams, K. F., Jr. (1995). Antiarrhythmic action of pharmacological administration of magnesium in heart failure: a critical review of new data. *Magnes. Res.* **8**, 389-401.

Taylor, K. M., Morgan, H. E., Johnson, A. and Nicholson, R. I. (2004). Structure-function analysis of HKE4, a member of the new LIV-1 subfamily of zinc transporters. *Biochem. J.* **377**, 131-139.

Thelen, M., Fehr, S., Schweizer, M., Braulke, T. and Galliciotti, G. (2012a). High expression of disease-related Cln6 in the cerebral cortex, purkinje cells, dentate gyrus, and hippocampal ca1 neurons. *J. Neurosci. Res.* **90**, 568-574.

Thelen, M., Damme, M., Schweizer, M., Hagel, C., Wong, A. M., Cooper, J. D., Braulke, T. and Galliciotti, G. (2012b). Disruption of the autophagy-lysosome pathway is involved in neuropathology of the nclf mouse model of neuronal ceroid lipofuscinosis. *PLoS ONE* **7**, e35493.

Uusi-Rauva, K., Luiro, K., Tanhuanpää, K., Kopra, O., Martín-Vasallo, P., Kyttälä, A. and Jalanko, A. (2008). Novel interactions of CLN3 protein link Batten disease to dysregulation of fodrin-Na+, K+ ATPase complex. *Exp. Cell Res.* **314**, 2895-2905.

Wang, C. Y., Jenkitkasemwong, S., Duarte, S., Sparkman, B. K., Shawki, A., Mackenzie, B. and Knutson, M. D. (2012). ZIP8 is an iron and zinc transporter whose cell-surface expression is up-regulated by cellular iron loading. *J. Biol. Chem.* **287**, 34032-34043.

Weimer, J. M., Benedict, J. W., Getty, A. L., Pontikis, C. C., Lim, M. J., Cooper, J. D. and Pearce, D. A. (2009). Cerebellar defects in a mouse model of juvenile neuronal ceroid lipofuscinosis. *Brain Res.* **1266**, 93-107.